

CrossMark
click for updates

Cite this: DOI: 10.1039/c6cp08125h

The decomposition of benzenesulfonyl azide: a matrix isolation and computational study†

Guohai Deng,^a Xuelin Dong,^a Qifan Liu,^a Dingqing Li,^a Hongmin Li,^a Qiao Sun^b and Xiaoqing Zeng^{*a}

The thermal-decomposition and photo-decomposition of benzenesulfonyl azide, PhS(O)₂N₃, have been studied by combining matrix-isolation IR spectroscopy and quantum chemical calculations. Upon flash vacuum pyrolysis at 800 K, the azide splits off molecular nitrogen and exclusively furnishes phenylnitrene (PhN) and SO₂ in the gas phase. In contrast, the azide favors stepwise photodecomposition in solid Ar and Ne matrices at 2.8 K. Specifically, the UV laser photolysis (193 and 266 nm) of PhS(O)₂N₃ results in the formation of the key nitrene intermediate PhS(O)₂N in the triplet ground state, which undergoes pseudo-Curtius rearrangement into *N*-sulfonyl imine PhNSO₂ under subsequent visible light irradiation (380–450 nm). Further fragmentation of PhNSO₂ into SO₂ and PhN followed by ring-expansion to dihydroazepine also occurs upon visible light irradiation. The preference of the stepwise mechanism for the decomposition of PhS(O)₂N₃ is supported by quantum chemical calculations using DFT B3LYP/6-311++G(3df,3pd) and CBS-QB3 methods.

Received 28th November 2016,
Accepted 11th January 2017

DOI: 10.1039/c6cp08125h

www.rsc.org/pccp

Introduction

Covalent azides R–N₃ are versatile reagents that have been broadly used such as in cycloaddition reactions in chemistry and biology,^{1a} synthesis of high-energy density polynitrogen materials,^{1b} and surface functionalization of nanomaterials.^{1c} Generally, covalent azides are energetic and sensitive to heat and irradiation due to the facile elimination of molecular nitrogen and simultaneous formation of a highly reactive nitrene intermediate R–N, which may undergo further inter- or intramolecular reactions under the decomposition conditions. As an alternative route, concerted decomposition of azide into N₂ and the rearrangement product may occur without the intermediacy of nitrene. The mechanism for the decomposition of covalent azides and also the properties of the involved nitrene intermediates have been extensively studied from both experimental and theoretical points of view.²

As one of the best known reactions in organic chemistry, the Curtius-rearrangement refers to the decomposition of carbonyl azide RC(O)N₃ into isocyanate RNCO with concomitant N₂ elimination.³ The mechanism for the decomposition of various carbonyl azides (*e.g.*, HC(O)N₃,⁴ CH₃C(O)N₃,⁵ CH₃OC(O)N₃,⁶

and PhC(O)N₃,⁷) keeps attracting attention in the field of physical organic chemistry. By analogy, a similar rearrangement reaction, known as the pseudo-Curtius rearrangement, has been extended to other structurally related α -oxo azides, including phosphoryl azide R₂P(O)N₃,⁸ sulfinyl azide RS(O)N₃,⁹ and sulfonyl azide RS(O)₂N₃.¹⁰ Sulfonyl azides are useful starting materials for the synthesis of biologically active enamines, amidines, and amidates.¹¹ Similar to the decomposition of carbonyl azides, sulfonyl azides RS(O)₂N₃ may undergo pseudo-Curtius rearrangement into *N*-sulfonyl imine RNSO₂ *via* the sulfonyl nitrene intermediate RS(O)₂N. However, the early solution chemistry¹² and more recent time-resolved spectroscopy studies^{10a,b} upon both the thermal-decomposition and photo-decomposition of sulfonyl azides failed to obtain convincing evidence for the formation of the final rearrangement product RNSO₂, although a number of sulfonyl nitrene intermediates had been either directly detected or chemically trapped.

The decomposition of arylsulfonyl azides ArS(O)₂N₃ in solution was found to be rather complex. According to the previous solution studies,¹³ thermolysis and photolysis of arylsulfonyl azides in solvents produce traces of SO₂ and derivatives of the nitrene ArS(O)₂N. Later on, the photochemistry of 4-methylbenzenesulfonyl azide,¹⁴ 2-naphthylsulfonyl azide,^{10b,15} and *p*-bromophenylsulfonyl and *p*-tolylsulfonyl azides^{10a} was explored by joint laser flash photolysis and ultrafast spectroscopy. The corresponding arylsulfonyl nitrenes have been directly detected; however, the kinetics results demonstrate that the rearrangement proceeds in a concerted pathway *via* the “rearrangement in the excited state (RIES)” mechanism.

^a College of Chemistry, Chemical Engineering and Materials Science, Soochow University, 215123 Suzhou, P. R. China. E-mail: xqzeng@suda.edu.cn

^b School for Radiological and Interdisciplinary Sciences, Soochow University, 215123 Suzhou, P. R. China

† Electronic supplementary information (ESI) available: Calculated IR spectroscopic data, energies, and coordinates for all species discussed in the paper. See DOI: 10.1039/c6cp08125h

The photochemistry (265 nm, mercury lamp) of the parent arylsulfonyl azide, PhS(O)₂N₃, has been studied by Sheridan and Rempala in a solid N₂ matrix at 16 K,¹⁶ and the pseudo-Curtius rearrangement product PhNSO₂ with two IR bands at 1371 and 1323 cm⁻¹ was tentatively identified due to spectral congestion.

Very recently, the decomposition reactions of the simple sulfonyl azides RS(O)₂N₃ (R = F,^{10c} CH₃,¹⁷ CF₃,¹⁸ and CH₃O^{10d}) have been investigated by combining matrix isolation and quantum chemical calculations. All the corresponding sulfonyl nitrenes, generated from the photolysis of the azides in cryogenic matrices, have been directly observed in the triplet ground state, and the respective pseudo-Curtius rearrangement products were always accompanied only as minor photolysis products. However, owing to the very different reactivity of the initially generated sulfonyl nitrenes, diverse secondary reactions including rearrangement, dimerization, and fragmentation have been observed, through which novel sulfur-containing species FSO₂,^{10c} NSO₂,^{18a} and HNSO₂^{10d} have been produced in the gas phase.

Herein, the thermal-decomposition and photo-decomposition of the simplest arylsulfonyl azide PhS(O)₂N₃ have been studied by combining matrix isolation IR spectroscopy and quantum chemical calculations. A stepwise decomposition pathway *via* the intermediacy of PhS(O)₂N and PhNSO₂ into PhN, SO₂, and N₂ was unambiguously established from both experimental and theoretical points of view.

Experimental section

Caution! Covalent azides are hazardous and explosive! Although no explosions occurred during this work, safety precautions (face shields, leather gloves, and protective leather clothing) are strongly recommended, particularly in the case of handling pure PhS(O)₂N₃ in the condensed phase.

Sample preparation

Benzenesulfonyl azide PhS(O)₂N₃ was prepared by the reaction of benzenesulfonyl chloride PhS(O)₂Cl with sodium azide (NaN₃) in acetone according to the reported procedure.¹⁹ The quality of the sample was checked by ¹H, ¹³C NMR spectroscopy (Bruker 400 MHz) and Raman spectroscopy (Horiba JY HR800).

Matrix IR spectroscopy

Matrix IR spectra were recorded on a FT-IR spectrometer (Bruker 70 V) in a reflectance mode using a transfer optic. A KBr beam splitter and a liquid-nitrogen-cooled MCT detector were used in the mid-IR region (4000–600 cm⁻¹). For each spectrum, 200 scans at a resolution of 0.5 cm⁻¹ were co-added.

The gaseous sample was mixed by passing a flow of matrix gas (Ne and Ar) through a cold U-trap (3–6 °C) containing *ca.* 20 mg of the azide. The azide/noble gas mixture (1:1000 estimated) was passed through Al₂O₃ (o.d. 2.0 mm, i.d. 1.0 mm), which could be heated over a length of approximately 25 mm by a tantalum wire (o.d. 0.4 mm, resistance 0.4 Ω). Then, the mixture was immediately deposited (2 mmol h⁻¹) onto the

Rh-plated copper block matrix support (2.8 K) under high vacuum (~10⁻⁶ Pa), using a closed-cycle helium cryostat (Sumitomo Heavy Industries, SRDK-408D2-F50H) inside the vacuum chamber. For the IR spectral measurement, the cryostat was horizontally rotated (180°) to allow the matrix-isolated sample under the irradiation of the IR beam. The electric power (voltage/current) used in pyrolysis experiments was 3.5 V/2.86 A. Photolysis was performed using an ArF excimer laser (Gamlaser EX5/250, 3 Hz, 193 nm), Nd³⁺:YAG laser (266 nm, MP-L-266, 10 mW), and a high-power flashlight (Boyu T648, 20 W).

Computational details

Geometry optimization and harmonic IR frequency (unscaled) calculations were performed using DFT methods (B3LYP,²⁰ M06-2X,²¹ MPW1PW91²²) combined with the 6-311++G(3df,3pd) basis set.²³ Accurate energies of the species were further calculated by using the complete basis set (CBS-QB3).²⁴ Time-dependent (TD)²⁵ B3LYP/6-311++G(3df,3pd) calculations were carried out for the prediction of UV-vis transitions. Local minima were confirmed by vibrational frequency analysis, and transition states were further confirmed by intrinsic reaction coordinate (IRC) calculations.²⁶ All calculations were performed using the Gaussian 09 suite of programs.²⁷

Results and discussion

Characterization of PhS(O)₂N₃

Despite the fact that the first synthesis of PhS(O)₂N₃ was reported in 1955,²⁸ it was only partially characterized by ¹H and ¹³C NMR and IR spectroscopy.¹⁹ We obtained the matrix-isolation (Ne and Ar) IR and Raman spectra of the azide (Fig. 1 with molecular structure), and the vibrational data (Table 1) were analyzed with the aid of quantum chemical calculations by using the B3LYP and M06-2X methods.

Generally, the experimentally observed IR spectra (Fig. 1B) of PhS(O)₂N₃ are in agreement with the DFT calculations (Fig. 1A).

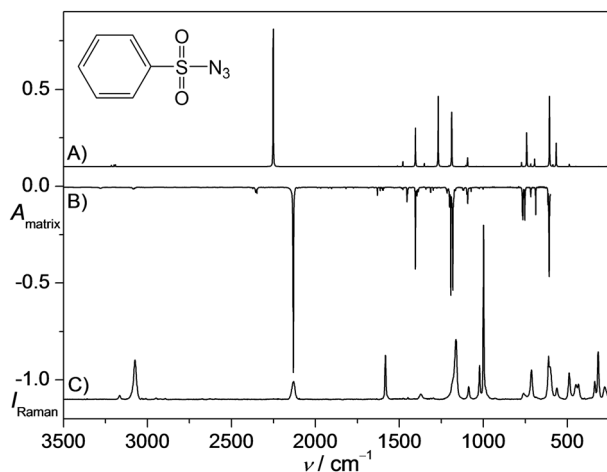


Fig. 1 (A) Calculated IR spectrum of PhS(O)₂N₃ at the B3LYP/6-311++G(3df,3pd) level; (B) the observed IR spectrum of PhS(O)₂N₃ in the solid Ne matrix at 2.8 K (absorbance *A*, resolution 0.5 cm⁻¹); (C) Raman spectrum of liquid PhS(O)₂N₃ at 298 K (Raman intensity *I*, resolution 2 cm⁻¹).

Table 1 Observed and calculated IR frequencies (cm^{-1}) for $\text{PhS(O)}_2\text{N}_3$ ^a

Observed ^b				Calculated ^c		
IR (Ne matrix)	IR (Ar matrix)	IR (liquid) ^e	Raman (liquid)	B3LYP	M06-2X	Approximate assignment ^d
3281.9 vw	3280.5 vw	3276 w		3215 (5)	3209 (6)	$\nu(\text{CH})$
			3166 w	3214 (<1)	3205 (<1)	$\nu(\text{CH})$
3084.9 vw	3080.6 vw	3069 w	3075 m	3199 (6)	3198 (<1)	$\nu(\text{CH})$
				3190 (7)	3192 (4)	$\nu(\text{CH})$
				3178 (<1)	3181 (<1)	$\nu(\text{CH})$
2131.7 vs	2129.0 vs	2129 s	2131 m	2251 (554)	2348 (515)	$\nu_{\text{as}}(\text{N}_3)$
1591.8 w	1589.7 w	1584 w	1588 m	1622 (2)	1661 (2)	$\nu(\text{CC})$
				1621 (<1)	1658 (<1)	$\rho(\text{CH})$
1479.2 w	1478.0 w	1477 w		1511 (4)	1519 (3)	$\rho(\text{CH})$
1454.9 w	1452.7 w	1450 m	1449 vw	1479 (21)	1488 (29)	$\rho(\text{CH})$
1405.2 s	1397.2 s	1372 s	1371 w	1404 (152)	1450 (164)	$\nu_{\text{as}}(\text{SO}_2)$
1341.9 vw	1341.2 vw			1351 (12)	1342 (9)	$\rho(\text{CH})$
1314.4 vw	1312.5 vw	1313 w		1330 (2)	1326 (<1)	$\rho(\text{CH})$
1298.6 w	1297.8 w	1298 w		1269 (244)	1279 (267)	$\nu_{\text{s}}(\text{N}_3)$
1194.5 s	1194.1 s		1185 w, sh	1204 (4)	1231 (268)	$\rho(\text{CH})$
1182.3 s	1180.5 s	1170 s	1162 s	1189 (143)	1200 (7)	$\nu_{\text{s}}(\text{SO}_2)$
				1188 (<1)	1177 (<1)	$\rho(\text{CH})$
1118.3 vw	1119.4 vw			1104 (5)	1124 (36)	$\rho(\text{CH})$
1093.4 w	1091.9 w	1088 m	1087 w	1094 (31)	1110 (5)	$\nu(\text{SC}) + \rho(\text{CH})$
1025.5 vw	1024.6 vw	1023 w	1023 m	1041 (1)	1056 (1)	Ring distortion
				1024 (<1)	1038 (<1)	Ring distortion
				1006 (<1)	1016 (<1)	$\omega(\text{CH})$
1002.4 vw	1000.9 vw	1000 w	998 vs	1000 (2)	1005 (1)	Ring breathing
				958 (<1)	967 (<1)	$\omega(\text{CH})$
				865 (<1)	874 (<1)	$\omega(\text{CH})$
765.2 vw	764.0 vw		761 w	773 (15)	803 (121)	$\nu(\text{SN})$
753.4 s	751.4 s	751 m		742 (122)	778 (25)	$\nu(\text{SC})$
716.9 vw	715.1 vw		713 m	717 (11)	735 (44)	$\delta(\text{CH})$
688.1 w	686.5 w	685 m		695 (32)	703 (39)	$\delta(\text{CH})$
			612 m	627 (<1)	635 (183)	$\delta(\text{CH})$
607.9 s	603.9 s	601 s	563 w	606 (259)	624 (36)	$\nu(\text{SN}) + \delta(\text{SO}_2)$
		564 s		586 (8)	623 (7)	$\delta_{\text{o.o.p.}}(\text{N}_3)$
				566 (86)	581 (93)	$\nu(\text{SN}) + \delta(\text{SO}_2)$

^a A full list of the calculated harmonic IR frequencies (unscaled) is given in Table S1 in the ESI. ^b Band intensities: vs, very strong; s, strong; m, medium strong; w, weak; vw, very weak; sh, shoulder. ^c Calculated IR frequencies and intensities (km mol^{-1}) in parentheses with the 6-311++G(3df,3pd) basis set. ^d Tentative assignment based on the calculated vibrational displacement vectors. ^e Taken from ref. 19.

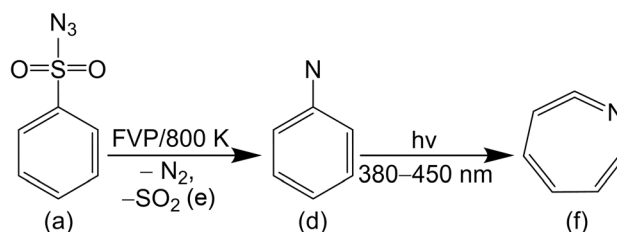
The band positions of $\text{PhS(O)}_2\text{N}_3$ observed in cryogenic matrices are very close to those in the liquid, except for the two SO_2 stretching vibrational modes. In a solid Ne matrix, the asymmetric and symmetric stretching modes appear at 1405.2 and 1182.3 cm^{-1} , whereas in the liquid these two shift to 1372 and 1170 cm^{-1} in the IR and 1371 and 1162 cm^{-1} in the Raman spectra, respectively. Very similar changes have also been observed for the same vibrational modes in $\text{CH}_3\text{S(O)}_2\text{N}_3$ (Ar matrix IR: $\nu_{\text{asym}}(\text{SO}_2)$ 1391.5 cm^{-1} , $\nu_{\text{sym}}(\text{SO}_2)$ 1180.0 cm^{-1} ; solid Raman: $\nu_{\text{asym}}(\text{SO}_2)$ 1357 cm^{-1} , $\nu_{\text{sym}}(\text{SO}_2)$ 1151 cm^{-1}).¹⁷ The red-shifts indicate intermolecular hydrogen bonding interactions with the SO_2 moiety in the condensed phase as have been observed in $\text{CH}_3\text{S(O)}_2\text{N}_3$ ($\text{H}_2\text{C}-\text{H} \cdots \text{OSO}$) by X-ray crystallography.¹⁷

The most characteristic asymmetric stretching vibration mode of the N_3 group in $\text{PhS(O)}_2\text{N}_3$ locates at 2131.7 cm^{-1} (Ne matrix). It is slightly red-shifted in comparison to those of other sulfonyl azides $\text{CH}_3\text{S(O)}_2\text{N}_3$ (2138.6 cm^{-1}),¹⁷ $\text{FS(O)}_2\text{N}_3$ (2162.3 cm^{-1}) and $\text{CF}_3\text{S(O)}_2\text{N}_3$ (2151.6 cm^{-1}).²⁹ According to the calculated vibrational displacement vectors, the symmetric N_3 stretching mode should appear as a strong IR band due to the large IR intensity (244 km mol^{-1} , B3LYP/6-311++G(3df,3pd)). However, only weak bands at 1298.6 (Ne matrix) and 1298 cm^{-1} (liquid) are found in the IR spectra. In contrast, the predicted

weak band for the C–H rocking mode ($\rho(\text{CH})$) occurs as a strong IR band at 1194.5 cm^{-1} . The discrepancies are probably caused by anharmonic vibrational coupling between these two modes. The C–S stretching vibration appears at 753.4 cm^{-1} , which is close to those in $\text{CH}_3\text{S(O)}_2\text{N}_3$ (731.7 cm^{-1})¹⁷ and $\text{CF}_3\text{S(O)}_2\text{N}_3$ (756.6 cm^{-1}).²⁹

Flash vacuum pyrolysis of $\text{PhS(O)}_2\text{N}_3$

The pyrolysis of $\text{PhS(O)}_2\text{N}_3$ (Scheme 1) was carried out by passing the azide/noble gas mixture (1 : 1000) through a heated Al_2O_3 furnace (ca. 800 K). The resulting mixture was immediately deposited onto the matrix support (2.8 K) for the IR spectroscopy study.



Scheme 1 Thermal decomposition of $\text{PhS(O)}_2\text{N}_3$ and photochemistry of PhN.

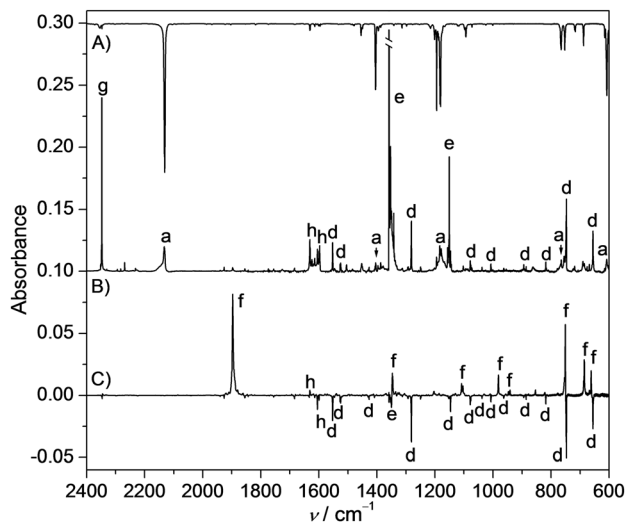


Fig. 2 (A) IR spectrum of $\text{PhS(O)}_2\text{N}_3$ in the solid Ne matrix at 2.8 K. (B) IR spectrum of the flash vacuum pyrolysis of $\text{PhS(O)}_2\text{N}_3$ in the solid Ne matrix at 2.8 K; (C) IR difference spectrum showing the change of the matrix containing flash vacuum pyrolysis products of $\text{PhS(O)}_2\text{N}_3$ upon visible light ($\lambda = 380\text{--}450\text{ nm}$, 20 W, 5 min) irradiation, bands for the depleted species point downwards and bands for the formed species point upwards. The IR bands of $\text{PhS(O)}_2\text{N}_3$ (a), PhN (d), SO_2 (e), cyclic $\text{C}_6\text{H}_5\text{N}$ (f), CO_2 (g), and H_2O (h) are labeled.

A typical IR spectrum of the pyrolysis products in the solid Ne matrix at 2.8 K is shown in Fig. 2B.

Compared to the IR spectrum of the starting material $\text{PhS(O)}_2\text{N}_3$ (Fig. 2A), almost 90% of the azide decomposes at 800 K. As a result, SO_2 (e, 1358.6 cm^{-1} and 1151.0 cm^{-1})³⁰ and PhN (d, 1683.6 , 1552.6 , 1525.6 , 1428.1 , 1408.5 , 1312.3 , 1280.8 , 1249.3 , 1146.1 , 1078.5 , 1008.2 , 963.3 , 885.9 , 819.1 , 747.5 , 655.4 cm^{-1})³¹ were identified by IR spectroscopy as the dominant pyrolysis products. To further prove the identification of PhN, subsequent irradiation of the matrix with visible light ($\lambda = 380\text{--}450\text{ nm}$) was applied. The corresponding IR difference spectrum (Fig. 2C) shows the exclusive depletion of PhN (d) and the formation of didehydroazepine (f, cyclic $\text{C}_6\text{H}_5\text{N}$). The same photo-induced ring expansion for PhN has been usually observed during the photolysis of phenyl azide in noble gas matrices.³¹

Therefore, the thermal decomposition of $\text{PhS(O)}_2\text{N}_3$ is very different from those of $\text{FS(O)}_2\text{N}_3$,^{10c} $\text{CF}_3\text{S(O)}_2\text{N}_3$,^{18a} and $\text{CH}_3\text{OS(O)}_2\text{N}_3$.^{10d} In addition to the common IR inactive product N_2 , mainly the thermally persistent sulfonyl nitrene $\text{FS(O)}_2\text{N}$ was obtained in the FVP of $\text{FS(O)}_2\text{N}_3$. As for $\text{CF}_3\text{S(O)}_2\text{N}_3$, the thermolysis products were found to be CF_3 and NSO_2 . Whereas CH_2O and HNSO_2 were identified by IR spectroscopy for $\text{CH}_3\text{OS(O)}_2\text{N}_3$. Two possible pathways leading to the formation of PhN, SO_2 , and N_2 from $\text{PhS(O)}_2\text{N}_3$ might be involved. One is the concerted migration of the N_3 group and elimination of the SO_2 moiety. Then, as the key intermediate species, phenylazide (PhN_3) should be generated followed by its complete decomposition into PhN and N_2 under the pyrolysis conditions. However, according to the latest study of the flash vacuum pyrolysis of PhN_3 , some of the azide can survive at 800 K.³² The absence of the IR bands for PhN₃

in the IR spectrum of the FVP products of $\text{PhS(O)}_2\text{N}_3$ renders this route unlikely.

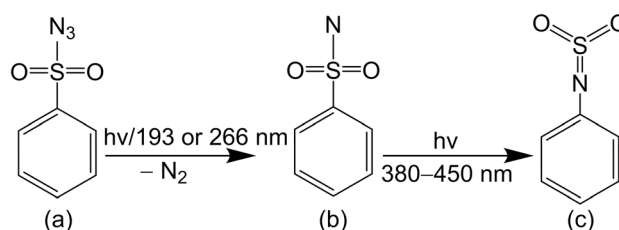
As an alternative pathway, the decomposition of $\text{PhS(O)}_2\text{N}_3$ may proceed by spitting off N_2 and forming the nitrene intermediate $\text{PhS(O)}_2\text{N}$, which can either isomerize into PhNSO_2 followed by N–S bond cleavage into PhN and SO_2 , or directly dissociate into PhN and SO_2 concertedly. This assumption is partially supported by the observation of the trapping products of arylsulfonyl nitrenes during the thermolysis of arylsulfonyl azides in aprotic solvents.^{13a} However, the nitrene $\text{PhS(O)}_2\text{N}$ was not experimentally observed among the pyrolysis products. Thus, it is very likely that the initially generated nitrene $\text{PhS(O)}_2\text{N}$ in the gas phase is unstable against fragmentation under the pyrolysis conditions.

Photodecomposition of $\text{PhS(O)}_2\text{N}_3$

To capture the decomposition intermediate, the photochemistry of $\text{PhS(O)}_2\text{N}_3$ (Scheme 2) in noble gas matrices (Ar, Ne) at 2.8 K was studied by utilizing an ArF excimer laser (193 nm), which was proved to be powerful in producing various missing α -oxo nitrenes in cryogenic matrices through photolysis of the azide precursors.³³

The IR difference spectrum reflecting the change of the matrix-isolated azide upon irradiation is shown in Fig. 3B. Unlike the aforementioned FVP of $\text{PhS(O)}_2\text{N}_3$, neither PhN nor SO_2 but a new species with one set of IR bands at 1588.7 , 1452.5 , 1348.9 , 1168.2 , 1090.8 , 1000.2 , 766.7 , 736.7 , and 683.7 cm^{-1} was generated upon irradiation. To aid the assignment, theoretical calculations on the IR frequencies for the most likely candidate species, benzenesulfonyl nitrene ($\text{PhS(O)}_2\text{N}$), in both singlet and triplet states were performed, and the results are summarized in Table 2. Clearly, the calculated spectrum for the lower-energy triplet species (Fig. 3D) shows better agreement with the experimental data. The two most intense bands at 1348.9 and 1168.2 cm^{-1} belong to the asymmetric and symmetric SO_2 stretching modes, respectively, which are close to those in $\text{PhS(O)}_2\text{N}_3$ (1405.2 and 1182.3 cm^{-1}), $\text{CF}_3\text{S(O)}_2\text{N}$ (1389.8 and 1179.8 cm^{-1}),^{18b} and $\text{CH}_3\text{S(O)}_2\text{N}$ (1349.8 and 1156.6 cm^{-1}).¹⁷ The S–N stretching mode appears at 736.7 cm^{-1} , which is also close to that in $\text{CF}_3\text{S(O)}_2\text{N}$ (723.2 cm^{-1}).^{18b}

According to the TD-B3LYP/6-311++G(3df,3pd) calculation (Table S3 in the ESI[†]), triplet $\text{PhS(O)}_2\text{N}$ is expected to absorb visible light with predicted vertical transition at 425 nm ($f = 0.054$). Therefore, the matrix containing the 193 nm laser photolysis products of $\text{PhS(O)}_2\text{N}_3$ was further subjected to



Scheme 2 Photodecomposition of $\text{PhS(O)}_2\text{N}_3$ and photochemistry of $\text{PhS(O)}_2\text{N}$.

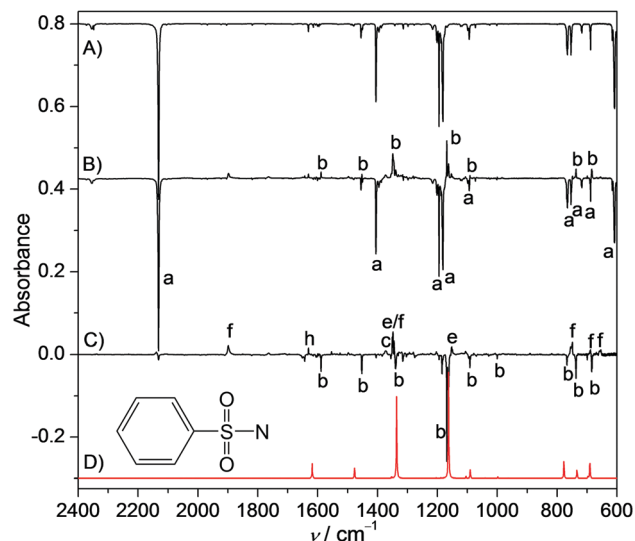


Fig. 3 (A) IR spectrum of $\text{PhS}(\text{O})_2\text{N}_3$ in the solid Ne matrix at 2.8 K; (B) IR difference spectrum showing the change of $\text{PhS}(\text{O})_2\text{N}_3$ in the solid Ne matrix upon the 193 nm laser photolysis (3 Hz, 5 mJ, 10 min); (C) IR difference spectrum showing the change of the matrix upon subsequent visible light irradiation ($\lambda = 380\text{--}450$ nm, 20 W, 5 min), bands for the depleted species point downwards and bands for the formed species point upwards; (D) calculated IR spectrum of triplet $\text{PhS}(\text{O})_2\text{N}$ at the UB3LYP/6-311++G(3df,3pd) level. The IR bands of $\text{PhS}(\text{O})_2\text{N}_3$ (a), $\text{PhS}(\text{O})_2\text{N}$ (b), PhNSO_2 (c), SO_2 (e), cyclic $\text{C}_6\text{H}_5\text{N}$ (f), and H_2O (h) are labeled.

visible light irradiation (380–450 nm). All the IR bands of $\text{PhS}(\text{O})_2\text{N}$ (b) vanished completely, and SO_2 (e) and cyclic $\text{C}_6\text{H}_5\text{N}$ (f) were produced (Fig. 3C). Additionally, a new carrier with a weak but distinguishable band at 1372.7 cm^{-1} (c) was formed after irradiation. The band position is very close to the predicted strongest IR band at 1376 cm^{-1} for the SO_2 asymmetric stretching mode in the expected pseudo-Curtius rearrangement product PhNSO_2 (Table S4 in the ESI[†]). However, the attempt to increase the abundance of the carrier for this band upon prolonged 193 nm laser irradiation of the azide was unsuccessful.

Considering the existence of two UV absorption bands at 270 and 200 nm for $\text{PhS}(\text{O})_2\text{N}_3$, a 266 nm laser was also used for the photolysis of the azide. The IR difference spectra showing the changes of the azide in a solid Ar matrix after the successive 266 nm laser and visible light (380–450 nm) irradiation are Fig. 4B and C, respectively. For comparison, the theoretically predicted IR spectrum of PhNSO_2 at the B3LYP/6-311++G(3df,3pd) level is also depicted (Fig. 4D).

Similar to the 193 nm laser irradiation, the 266 nm laser irradiation caused efficient depletion of the azide and formation of the sulfonyl nitrene $\text{PhS}(\text{O})_2\text{N}$ (b, 1586.6 , 1450.4 , 1336.3 , 1160.6 , 1087.6 , 999.9 , 765.9 , 737.3 , and 682.5 cm^{-1}). In contrast, the subsequent visible light irradiation enables much more confident identification of the IR bands for PhNSO_2 (c). In addition to the band at 1367.1 cm^{-1} (1372.7 cm^{-1} in Ne matrix), several weaker bands at 1484.6 , 1328.6 , 1280.3 , 1190.4 , 1005.8 , 758.0 , and 686.9 cm^{-1} were found to be associated with the same carrier (Fig. 4C). The band positions are in good agreement with the calculated values at 1520 , 1376 , 1349 , 1310 , 1189 , 1013 , 775 ,

Table 2 Observed and calculated IR frequencies (cm^{-1}) of $\text{PhS}(\text{O})_2\text{N}^a$

Observed ^b		Calculated ^c		Approximate assignment ^d
Ne matrix	Ar matrix	B3LYP	M06-2X	
		3215 (7)	3220 (7)	$\nu(\text{CH})$
		3214 (<1)	3218 (<1)	$\nu(\text{CH})$
		3199 (5)	3208 (<1)	$\nu(\text{CH})$
		3191 (7)	3203 (4)	$\nu(\text{CH})$
		3178 (<1)	3189 (<1)	$\nu(\text{CH})$
1588.7 m	1586.6 m	1618 (28)	1658 (<1)	$\nu(\text{CC})$
		1611 (<1)	1657 (15)	$\rho(\text{CH})$
		1507 (<1)	1519 (<1)	$\rho(\text{CH})$
1452.5 m	1450.4 m	1477 (18)	1492 (21)	$\rho(\text{CH})$
		1353 (2)	1427 (169)	$\rho(\text{CH})$
1348.9 s	1336.3 s	1336 (148)	1347 (14)	$\nu_{\text{as}}(\text{SO}_2)$
		1331 (<1)	1334 (<1)	$\rho(\text{CH})$
		1204 (<1)	1230 (210)	$\rho(\text{CH})$
		1189 (<1)	1205 (18)	$\rho(\text{CH})$
1168.2 vs	1160.6 vs	1163 (206)	1185 (<1)	$\nu_{\text{s}}(\text{SO}_2)$
		1104 (4)	1123 (28)	$\rho(\text{CH})$
1090.8 w	1087.6 w	1090 (16)	1114 (3)	$\nu(\text{SC}) + \rho(\text{CH})$
		1040 (<1)	1057 (<1)	Ring distortion
		1026 (<1)	1043 (<1)	Ring distortion
		1007 (<1)	1024 (<1)	$\omega(\text{CH})$
1000.2 vw	999.9 vw	998 (3)	1005 (<1)	Ring breathing
		963 (<1)	977 (<1)	$\omega(\text{CH})$
		864 (<1)	882 (<1)	$\omega(\text{CH})$
766.7 m	765.9 m	777 (30)	797 (12)	$\nu(\text{SC})$
736.7 w	737.3 m	734 (16)	763 (60)	$\nu(\text{SN})$
		697 (3)	721 (11)	$\delta(\text{CH})$
683.7 m	682.5 m	690 (30)	703 (30)	$\delta(\text{CH})$
		625 (<1)	622 (<1)	$\delta(\text{CH})$

^a A full list of the calculated harmonic IR frequencies (unscaled) is given in Table S2 of the ESI. ^b Band positions and intensities: vs, very strong; s, strong; m, medium strong; w, weak; vw, very weak. ^c Calculated with the 6-311++G(3df,3pd) basis set, IR intensities (km mol^{-1}) in parentheses. ^d Tentative assignment based on the calculated vibrational displacement vectors.

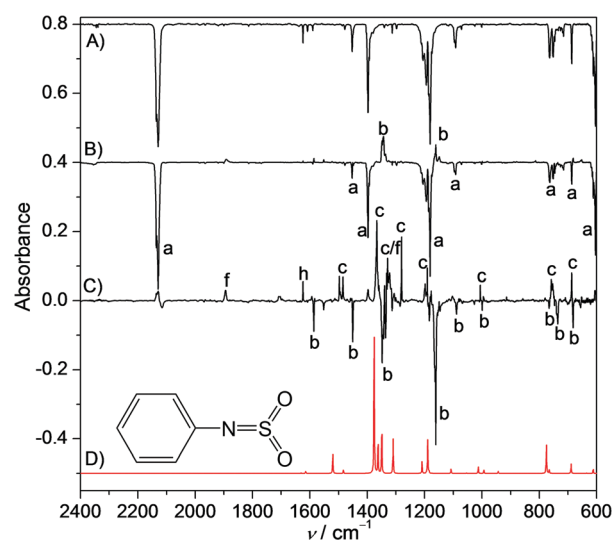


Fig. 4 (A) IR spectrum of $\text{PhS}(\text{O})_2\text{N}_3$ in the solid Ar matrix at 2.8 K; (B) IR difference spectrum showing the change of $\text{PhS}(\text{O})_2\text{N}_3$ in the solid Ar matrix upon 266 nm laser photolysis (10 mW, 10 min); (C) IR difference spectrum showing the change of the matrix upon subsequent visible light irradiation ($\lambda = 380\text{--}450$ nm, 20 W, 5 min), bands for the depleted species point downwards and bands for the formed species point upwards; (D) calculated IR spectrum of PhNSO_2 at the B3LYP/6-311++G(3df,3pd) level. The IR bands of $\text{PhS}(\text{O})_2\text{N}_3$ (a), $\text{PhS}(\text{O})_2\text{N}$ (b), PhNSO_2 (c), cyclic $\text{C}_6\text{H}_5\text{N}$ (f), and H_2O (h) are labeled.

and 689 cm^{-1} using the B3LYP/6-311++G(3df,3pd) method (Table S4 in the ESI†). Based on the calculated vibrational displacement vectors, the SO_2 asymmetric stretching vibration couples heavily with the ring breathing vibration and appears at 1005.8 cm^{-1} . It should be noted that the IR bands for PhNSO_2 (1367.1 and 1328.6 cm^{-1}) in the Ar matrix are quite close to the previously observed two bands at 1371 and 1323 cm^{-1} in the N_2 matrix during the 265 nm photolysis of $\text{PhS(O)}_2\text{N}_3$.¹⁶

The unambiguous identification of the IR bands for $\text{PhS(O)}_2\text{N}$ and PhNSO_2 clearly demonstrates that the stepwise Curtius rearrangement occurs during the photolysis of $\text{PhS(O)}_2\text{N}_3$ in cryogenic matrices (2.8 K). The absence of these two intermediates among the pyrolysis products suggests that they are probably not stable enough to survive under the pyrolysis conditions (800 K).

Quantum chemical calculation

To account for the mechanism, the potential energy surface (PES) for the decomposition of $\text{PhS(O)}_2\text{N}_3$ is computationally explored at the CBS-QB3 and B3LYP/6-311++G(3df,3pd) levels, and the results are summarized in Fig. 5.

Similar to the PESs of carbonyl azides,^{4a,5} two distinct pathways (stepwise *versus* concerted) for the pseudo-Curtius rearrangement of $\text{PhS(O)}_2\text{N}_3$ into PhNSO_2 and N_2 were computationally located. The activation barrier for the stepwise route to the nitrene $\text{PhS(O)}_2\text{N}$ and N_2 is 145 kJ mol^{-1} at the CBS-QB3 level, which is lower in energy than that for the concerted by 14 kJ mol^{-1} . As for the initially generated nitrene in the singlet state (^1A), there are three competing processes for its disappearance. One is the intersystem crossing (ISC) into the lower-energy triplet state (^3A). The singlet-triplet energy gap (ΔE_{ST}) is estimated to be 30 kJ mol^{-1} , which is very close to that of $\text{CH}_3\text{S(O)}_2\text{N}$ (34 kJ mol^{-1}) and $\text{CF}_3\text{S(O)}_2\text{N}$ (30 kJ mol^{-1}) at the same theoretical level.¹⁷ In fact, the ISC for $\text{PhS(O)}_2\text{N}$ can be extremely fast since the closely

related 2-naphthylsulfonyl nitrene^{10b} and *p*-tolylsulfonyl nitrene^{10a} were found to quickly relax from the singlet state into the longer-lived triplet state in CCl_4 with lifetimes of 700 ± 300 and $660 \pm 100\text{ ps}$, respectively, as determined by time-resolved infrared spectroscopy.

The second process refers to the intramolecular rearrangement from $\text{PhS(O)}_2\text{N}$ to PhNSO_2 , which needs to surmount a moderate barrier of 103 kJ mol^{-1} . More importantly, the latter is expected to be a thermally persistent species due to the extremely large C–N bond dissociation energy (BDE) of 336 kJ mol^{-1} ($\text{Ph-NSO}_2 \rightarrow \text{Ph} + \text{O}_2\text{SN}$). The absence of PhNSO_2 among the pyrolysis products confirms that no rearrangement occurred for the initially generated singlet nitrene even at 800 K .

The last possible process for singlet $\text{PhS(O)}_2\text{N}$ is the direct fragmentation of the C–S bond into the radical pair Ph and O_2SN . Although the BDE (82 kJ mol^{-1}) is even lower than the activation barrier for the rearrangement (103 kJ mol^{-1}), none of these two species was experimentally observed in the decomposition of the azide. Thus, it can be concluded that the prevailing channel for singlet $\text{PhS(O)}_2\text{N}$ is the spin relaxation into the triplet state, which is fully consistent with the observation of the triplet nitrene as the dominant photolysis products in the cryogenic matrices.

Despite the fact that the triplet nitrene can be trapped in cryogenic matrices, its metastability in the gas phase can be evidenced by the activation barrier of 94 kJ mol^{-1} for its rearrangement into triplet PhNSO_2 (Fig. 5). Unlike singlet PhNSO_2 , the triplet species is highly unstable because of the rather weak C–N bond with the BDE of merely 13 kJ mol^{-1} . Therefore, the complete dissociation fragments SO_2 , triplet PhN , and N_2 are expected to be obtained as the pyrolysis products of $\text{PhS(O)}_2\text{N}_3$, which is fully consistent with the experimental observation.

To gain more insight into the stability of the key nitrene intermediate $\text{PhS(O)}_2\text{N}$, the molecular structures in the singlet

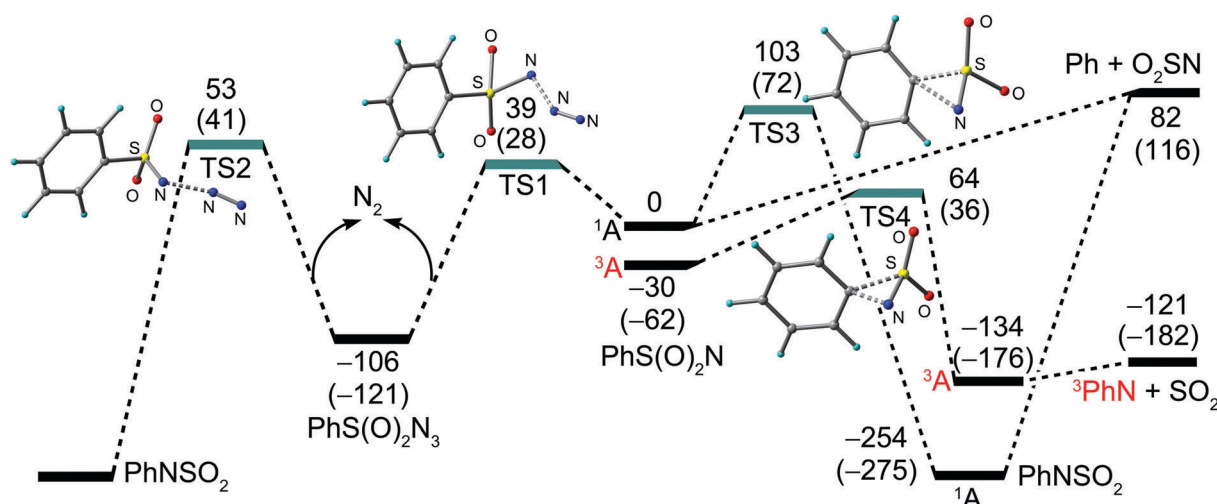


Fig. 5 Calculated potential energy surface for the decomposition of $\text{PhS(O)}_2\text{N}_3$ in the singlet state at the CBS-QB3 and B3LYP/6-311++G(3df,3pd) (in parentheses) levels of theory. The decomposition pathway of $\text{PhS(O)}_2\text{N}$ in the triplet state (in red colour) is also given. The relative energies are given in kJ mol^{-1} . The calculated molecular structures for the transition states are depicted. The symbols for nitrogen (blue), oxygen (red), and sulfur (yellow) atoms are shown, and the symbols for carbon (grey) and hydrogen (turquoise) atoms are omitted for clarity.

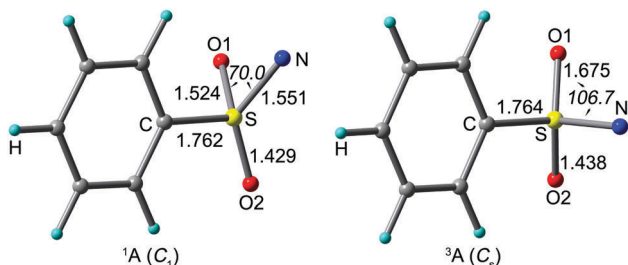


Fig. 6 Optimized structures of PhS(O)₂N in the singlet (¹A) and triplet (³A) states at the B3LYP/6-311++G(3df, 3pd) level of theory. Selected bond lengths [Å] and angles [°, in italics] are shown. The molecular symmetries are given in parentheses.

(¹A) and triplet (³A) states were optimized at the B3LYP/6-311++G(3df,3pd) level of theory. The key structural parameters are shown in Fig. 6. The most characteristic difference between the two spin states of PhS(O)₂N is the much narrower O–S–N angle in the singlet state (70.0°) than that in the triplet state (106.7°). Very similar differences have been found not only for other sulfonyl nitrenes like CF₃S(O)₂N (singlet: 72.2°; triplet: 107.9°)^{18b} and CH₃S(O)₂N (singlet: 70.7°; triplet: 106.6°)¹⁷ and also for other α-oxo nitrenes RC(O)N,⁵ R₂P(O)N,⁸ and RS(O)N.^{9b} The significant structural difference can be rationalized by an intramolecular interaction between the electron-deficient nitrene center and the adjacent oxygen atom (N···O), which stabilizes the closed-shell singlet by forming an oxazirine-like structure with the N···O distance of 1.767 Å. In sharp contrast, the N···O distance in the triplet state is 2.503 Å. Nevertheless, the triplet state remains as the ground state for PhS(O)₂N, whereas the closely related carbonyl analogue PhC(O)N prefers singlet multiplicity.⁷

Conclusions

Both thermal and photolytic decomposition reactions of the parent arylsulfonyl azide PhS(O)₂N₃ have been studied by combining matrix isolation IR spectroscopy and quantum chemical calculations. Upon flash vacuum pyrolysis at 800 K, the azide eliminates N₂ and exclusively furnishes SO₂ and PhN, which provides a new method for generating the important phenylnitrene in the gas phase. In contrast, laser photolysis (193 and 266 nm) of PhS(O)₂N₃ in cryogenic matrices enables the identification of the key nitrene intermediate PhS(O)₂N in the triplet ground state, which undergoes rearrangement into *N*-sulfonyl imine PhNSO₂ under visible light irradiation (380–450 nm). The identification of these two intermediates firmly supports the feasibility of stepwise Curtius rearrangement for arylsulfonyl azides *via* the corresponding nitrene intermediate.

Computationally, the potential energy surface (PES) for the decomposition of PhS(O)₂N₃ reveals the preference of the stepwise Curtius rearrangement *via* the intermediacy of PhS(O)₂N. However, the initially generated nitrene in the singlet state favors intersystem crossing to the triplet ground state, which may rearrange into PhNSO₂ on the triplet PES followed by immediate dissociation into the experimentally observed final thermal

decomposition products PhN and SO₂. The successful isolation of singlet PhNSO₂ from the photo-induced rearrangement of triplet PhS(O)₂N in solid noble gas matrices suggests the possible involvement of even short-lived excited state species under the photolysis conditions.

Acknowledgements

This work was supported by the National Natural Science Foundation of China (21422304, 21372173 and 21673147), the Priority Academic Program Development of Jiangsu Higher Education Institutions (PAPD) and the China Postdoctoral Science Foundation (2016M600436). The authors greatly acknowledge Professor Robert S. Sheridan for sharing the unpublished results.

References

- (a) S. Bräse and K. Banert, *Organic Azides: Syntheses and Applications*, John Wiley & Sons, Chichester, 2010; (b) P. Portius and M. Davis, *Coord. Chem. Rev.*, 2013, **257**, 1011; (c) L. H. Liu and M. D. Yan, *Acc. Chem. Res.*, 2010, **43**, 1434.
- (a) D. E. Falvery and A. D. Gudmundsdottir, *Nitrenes and Nitrenium Ions*, Wiley Series of Reactive Intermediates in Chemistry and Biology, John Wiley & Sons, Hoboken, 2013; (b) N. P. Gritsan, M. S. Platz and W. T. Borden, *The Study of Nitrenes by Theoretical Methods*, Taylor and Francis, Boca Raton, 2005; (c) R. A. Moss, M. S. Platz and M. Jones, Jr., *Reactive Intermediate Chemistry*, Wiley-Interscience, Hoboken, 2004.
- T. Curtius, *Ber. Dtsch. Chem. Ges.*, 1890, **23**, 3023.
- (a) K. Banert, C. Berndt, M. Hagedorn, H. Liu, T. Anacker, J. Friedrich and G. Rauhut, *Angew. Chem., Int. Ed.*, 2012, **51**, 4718; (b) X. Q. Zeng, E. Bernhardt, H. Beckers, K. Banert, M. Hagedorn and H. Liu, *Angew. Chem., Int. Ed.*, 2013, **52**, 3503, and references therein.
- J. Liu, S. Mandel, C. M. Hadad and M. S. Platz, *J. Org. Chem.*, 2004, **69**, 8583.
- (a) J. M. Dyke, G. Levita, A. Morris, J. S. Ogden, A. A. Dias, M. Algarra, J. P. Santos, M. L. Costa, P. Rodrigues, M. M. Andrade and M. T. Barros, *Chem. – Eur. J.*, 2005, **11**, 1665; (b) R. E. Wilde, T. K. K. Srinivasan and W. Lwowski, *J. Am. Chem. Soc.*, 1971, **93**, 860; (c) J. H. Teles and G. Maier, *Chem. Ber.*, 1989, **122**, 745.
- (a) E. A. Pritchina, N. P. Gritsan, A. Maltsev, T. Bally, T. Autrey, Y. L. Liu, Y. H. Wang and J. P. Toscano, *Phys. Chem. Chem. Phys.*, 2003, **5**, 1010; (b) C. Wentrup and H. Bornemann, *Eur. J. Org. Chem.*, 2005, 4521.
- (a) S. Vyas, S. Muthukrishnan, J. Kubicki, R. D. McCulla, G. Burdzinski, M. Sliwa, M. S. Platz and C. M. Hadad, *J. Am. Chem. Soc.*, 2010, **132**, 16796; (b) R. D. McCulla, G. A. Gohar, C. M. Hadad and M. S. Platz, *J. Org. Chem.*, 2007, **72**, 9426.
- (a) T. J. Maricich and V. L. Hoffman, *J. Am. Chem. Soc.*, 1974, **96**, 7770; (b) Z. Wu, D. Q. Li, H. M. Li, B. F. Zhu, H. L. Sun, J. S. Francisco and X. Q. Zeng, *Angew. Chem., Int. Ed.*, 2016,

- 55, 1507; (c) T. J. Maricich and C. N. Angeletakis, *J. Org. Chem.*, 1984, **49**, 1931.
- 10 (a) A. V. Kuzmin, C. Neumann, L. J. G. W. van Wilderen, B. A. Shainyan and J. Bredenbeck, *Phys. Chem. Chem. Phys.*, 2016, **18**, 8662; (b) J. Kubicki, H. L. Luk, Y. Zhang, S. Vyas, H. L. Peng, C. M. Hadad and M. S. Platz, *J. Am. Chem. Soc.*, 2012, **134**, 7036; (c) X. Q. Zeng, H. Beckers and H. Willner, *J. Am. Chem. Soc.*, 2013, **135**, 2096; (d) G. H. Deng, Z. Wu, D. Q. Li, R. Linguerri, J. S. Francisco and X. Q. Zeng, *J. Am. Chem. Soc.*, 2016, **138**, 11509.
- 11 (a) T. Miura, Y. Funakoshi, M. Morimoto, T. Biyajima and M. Murakami, *J. Am. Chem. Soc.*, 2012, **134**, 17440; (b) H. D. Xu, Z. H. Jia, K. Xu, M. Han, S. N. Jiang, J. Cao, J. C. Wang and M. H. Shen, *Angew. Chem., Int. Ed.*, 2014, **53**, 9284; (c) Y. D. Li, Y. D. Feng, L. H. Xu, L. H. Wang and X. L. Cui, *Org. Lett.*, 2016, **18**, 4924; (d) X. S. Xiao, C. Hou, Z. H. Zhang, Z. F. Ke, J. Y. Lan, H. F. Jiang and W. Zeng, *Angew. Chem., Int. Ed.*, 2016, **55**, 11897.
- 12 (a) M. T. Reagan and A. Nickon, *J. Am. Chem. Soc.*, 1968, **90**, 4096; (b) R. A. Abramovitch and R. G. Sutherland, *Top. Curr. Chem.*, 1970, **16**, 1; (c) R. A. Abramovitch and W. D. Holcomb, *Chem. Commun.*, 1969, 1298.
- 13 (a) W. Lwowski and E. Scheiffele, *J. Am. Chem. Soc.*, 1965, **87**, 4359; (b) R. A. Abramovitch, W. D. Holcomb and S. Wake, *J. Am. Chem. Soc.*, 1981, **103**, 1525; (c) D. S. Breslow, E. I. Edwards, E. C. Linsay and H. Omura, *J. Am. Chem. Soc.*, 1976, **98**, 4268.
- 14 J. C. Garay, V. Maloney, M. Marlow and P. Small, *J. Phys. Chem.*, 1996, **100**, 5788.
- 15 J. Kubicki, Y. L. Zhang, J. D. Xue, H. L. Luk and M. S. Platz, *Phys. Chem. Chem. Phys.*, 2012, **14**, 10377.
- 16 R. S. Sheridan and P. Rempala, Books of Abstracts, 217th ACS National Meeting, Anaheim, CA, American Chemical Society, Washington, DC, 1999; ORGN-287.
- 17 G. H. Deng, D. Q. Li, Z. Wu, H. M. Li, E. Bernhardt and X. Q. Zeng, *J. Phys. Chem. A*, 2016, **120**, 5590.
- 18 (a) X. Q. Zeng, H. Beckers and H. Willner, *Angew. Chem., Int. Ed.*, 2013, **52**, 7981; (b) X. Q. Zeng, H. Beckers, H. Willner, P. Neuhaus, D. Grote and W. Sander, *J. Phys. Chem. A*, 2015, **119**, 2281.
- 19 J. Waser, B. Gaspar, H. Nambu and E. M. Carreira, *J. Am. Chem. Soc.*, 2006, **128**, 11693.
- 20 A. D. Becke, *J. Chem. Phys.*, 1993, **98**, 5648.
- 21 Y. Zhao and D. G. Truhlar, *Theor. Chem. Acc.*, 2008, **120**, 215.
- 22 C. Adamo and V. Barone, *J. Chem. Phys.*, 1998, **108**, 664.
- 23 (a) T. Clark, J. Chandrasekhar, G. W. Spitznagel and P. V. R. Schleyer, *J. Comput. Chem.*, 2004, **4**, 294; (b) M. J. Frisch, J. A. Pople and J. S. Binkley, *J. Chem. Phys.*, 1984, **80**, 3265.
- 24 J. A. Montgomery, M. J. Frisch, J. W. Ochterski and G. A. Petersson, *J. Chem. Phys.*, 2000, **112**, 6532.
- 25 (a) R. E. Stratmann, G. E. Scuseria and M. J. Frisch, *J. Chem. Phys.*, 1998, **109**, 8218; (b) J. B. Foresman, M. Head-Gordon, J. A. Pople and M. J. Frisch, *J. Phys. Chem.*, 1992, **96**, 135.
- 26 (a) C. Gonzalez and H. B. Schlegel, *J. Chem. Phys.*, 1989, **90**, 2154; (b) C. Gonzalez and H. B. Schlegel, *J. Phys. Chem.*, 1990, **94**, 5523.
- 27 M. J. Frisch, G. W. Trucks, H. B. Schlegel, G. E. Scuseria, M. A. Robb, J. R. Cheeseman, G. Scalmani, V. Barone, B. Mennucci, G. A. Petersson, H. Nakatsuji, M. Caricato, X. Li, H. P. Hratchian, A. F. Izmaylov, J. Bloino, G. Zheng, J. L. Sonnenberg, M. Hada, M. Ehara, K. Toyota, R. Fukuda, J. Hasegawa, M. Ishida, T. Nakajima, Y. Honda, O. Kitao, H. Nakai, T. Vreven, J. J. A. Montgomery, J. E. Peralta, F. Ogliaro, M. Bearpark, J. J. Heyd, E. Brothers, K. N. Kudin, V. N. Staroverov, T. Keith, R. Kobayashi, J. Normand, K. Raghavachari, A. Rendell, J. C. Burant, S. S. Iyengar, J. Tomasi, M. Cossi, N. Rega, J. M. Millam, M. Klene, J. E. Knox, J. B. Cross, V. Bakken, C. Adamo, J. Jaramillo, R. Gomperts, R. E. Stratmann, O. Yazyev, A. J. Austin, R. Cammi, C. Pomelli, J. W. Ochterski, R. L. Martin, K. Morokuma, V. G. Zakrzewski, G. A. Voth, P. Salvador, J. J. Dannenberg, S. Dapprich, A. D. Daniels, Ö. Farkas, J. B. Foresman, J. V. Ortiz, J. Cioslowski and D. J. Fox, *Gaussian 09, Revision A.2*, Gaussian, Inc., Wallingford CT, 2009.
- 28 O. C. Dermer and M. T. Edmison, *J. Am. Chem. Soc.*, 1955, **77**, 70.
- 29 X. Q. Zeng, M. Gerken, H. Beckers and H. Willner, *J. Phys. Chem. A*, 2010, **114**, 7624.
- 30 X. Q. Zeng, H. Beckers, P. Neuhaus, D. Grote and W. Sander, *Z. Anorg. Allg. Chem.*, 2012, **638**, 526.
- 31 J. C. Hayes and R. S. Sheridan, *J. Am. Chem. Soc.*, 1990, **112**, 5879.
- 32 J. Mierse-Pérez, E. Mendez-Vega, K. Velappan and W. Sander, *J. Org. Chem.*, 2015, **80**, 11926.
- 33 H. M. Li, H. B. Wan, Z. Wu, D. Q. Li, D. Bégué, C. Wentrup and X. Q. Zeng, *Chem. – Eur. J.*, 2016, **22**, 7856, and references therein.